ELSEVIER

Thermochimica Acta 399 (2003) 225–239

thermochimica acta

www.elsevier.com/locate/tca

Kinetics of the oxidation of bismuth tellurite, Bi_2TeO_5 Empirical model and least squares evaluation strategies to obtain reliable kinetic information

Gábor Várhegyi [a], László Pöppl [b,*], István Földvári [c]

[a] *Research Laboratory of Materials and Environmental Chemistry, Chemical Research Center, Hungarian Academy of Sciences, P.O. Box 17, 1525 Budapest, Hungary*

[b] *Institute of Inorganic and Analytical Chemistry, Loránd Eötvös University, P.O. Box 32, 1518 Budapest 112, Hungary*

[c] *Research Institute for Solid State Physics and Optics, Hungarian Academy of Sciences, P.O. Box 49, 1525 Budapest 114, Hungary*

Received 11 June 2002; received in revised form 14 June 2002; accepted 1 September 2002

Abstract

The oxidation kinetics of Bi_2TeO_5, a special non-linear optical material, was investigated. Thermogravimetric (TG) experiments combining non-isothermal (1–10 °C/min) and isothermal (600–700 °C) sections at oxygen partial pressures of 21–101 kPa were evaluated. The model contained an empirical $f(\alpha)$ function to describe the dependence of the reaction rate on the fraction reacted (α). The unknown parameters were determined by the least-squares evaluation of 12 experiments. Different evaluation strategies were employed to ensure the reliability of the obtained kinetic information. A least-squares baseline correction method was also proposed. The results indicated that the reaction rate is highly influenced by the solid phase diffusion of the oxygen. Several combinations of the experimental conditions resulted in $f(\alpha)$ functions increasing to a maximum at $\alpha \approx 0.3$–0.5 while monotonously decreasing $f(\alpha)$ functions were observed in other cases. This behavior indicates that the size, variation and topography of the reaction surface depend on the experimental conditions.

Keywords: Bismuth tellurite; Thermogravimetry; Kinetics; Reaction surface; Diffusion control

1. Introduction

Bismuth tellurite, Bi_2TeO_5, is a special non-linear optical material. Its crystals exhibit a long-living photorefractive signal that develops in the four-wave mixing experiments without any fixing process and lasts for years in the dark [1,2]. In a recent work, the reaction $Bi_2TeO_5 + 1/2O_2 = Bi_2TeO_6$ was studied by thermogravimetric, microscopic and DSC experiments [3]. Using powdered Bi_2TeO_5 samples, the oxidation starts at about 450 °C but complete oxidation can only be achieved by long annealing of the samples in oxygen ambient at 670 °C. At higher temperatures the Bi_2TeO_6 decomposes. Optical microscopy on single crystals revealed that the reaction starts at selective sites of the surface from which cracks and channels develop.

The Bi_2TeO_5 crystals are grown from the melt in air and the oxidation kinetics appears to be an essential issue in the crystal quality. Accordingly, the aim of the present work is the kinetic analysis of the observations.

* Corresponding author. Tel.: +36-1-209-0609; fax: +36-1-209-0602.
E-mail address: poppl@para.chem.elte.hu (L. Pöppl).

0040-6031/02/$ – see front matter
PII: S0040-6031(02)00469-0

Nomenclature

α	reacted fraction of the sample
a	parameter of $f(\alpha)$ (see Eq. (2))
A	pre-exponential factor (s^{-1})
b	parameter of $f(\alpha)$ (see Eq. (2))
E	activation energy (kJ/mol)
F	normalizing factor for $f(\alpha)$ (see Eq. (2))
$f(\alpha)$	function expressing the dependence of the reaction rate on α
fit	$100s^{0.5}$ (%)
$m^{calc}(t)$	normalized sample mass calculated from the model
$m^{obs}(t)$	mass of the sample divided by the initial sample mass
$\delta m(t)$	baseline correction
N	number of evaluated data on an experimental curve
P_{O_2}	partial pressure of oxygen (kPa)
R	gas constant (8.3143×10^{-3} kJ mol^{-1} K^{-1})
s	least squares sum for one experiment
S	least squares sum for a series of experiments
t	time (s)
T	temperature (°C, K)
$T_{isothermal}$	temperature of an isothermal section (°C)
z	parameter of $f(\alpha)$ (see Eq. (2))

In thermal analysis, the kinetic evaluation is usually based on a model of type

$$\frac{d\alpha}{dt} = A \exp\left(\frac{-E}{RT}\right) f(\alpha) \quad (1)$$

where α is the reacted mole fraction, A the preexponential factor, E the activation energy, and $f(\alpha)$ is a function describing the dependence of the reaction rate on the conversion.

We shall briefly survey a few theoretically deduced $f(\alpha)$ functions, shown in Fig. 1, since they help the interpretation of the results presented in this paper. The first order kinetics, which is a simple technical approximation for several solid phase reactions, was also drawn for comparison. Convex and concave curves, falling below and above this straight line at higher conversion values, represent cases when the reaction is hindered or facilitated as the conversion proceeds.

If the reaction occurs on the external surface and the products form a layer blocking the access of the reactant gas, strong diffusion-control appears [4]. Fig. 1 shows three frequently used equations for diffusion controlled reactions: the Jander and the Ginstling–Brounshtein equations for three-dimensional diffusion and the two-dimensional diffusion model [4]. These functions start at $f(\alpha) = \infty$, hence we plotted them only in the domain of $0.05 \leq \alpha \leq 1$. It is interesting to observe the high similarity of these curves.

If the product layer does not form a barrier to the reactant gas, then the reaction rate is approximately proportional to the surface area. This situation results in characteristic concave curves. The cause of the concaveness is the increasing ratio of the reactive surface and the sample mass. The case when the reaction takes place on the external surface is represented by the well-known contracting sphere model [4] in Fig. 1. In many cases the reacting samples have considerable internal surface in the form of pores and capillaries. There are well-elaborated models for the burn-off of carbonaceous materials. Fig. 1 shows the random pore models of Bhatia and Perlmutter [5] with parameters presented by Su and Perlmutter [6].

Internal surface can also form through cracks and splits due to physical stress during the heating of the samples. This can help the growth of domains filled in by the product phase inside the sample. The irregularities on the boundary surfaces speed up the reaction. A similar process, based on the random formation of nuclei during the whole reaction, is represented by the well-known Avrami–Erofeev–Mampel model [4] in Fig. 1.

The thermoanalytical studies on the oxidation of inorganic compounds usually employs Eq. (1) with $f(\alpha)$ functions selected from the classical literature of thermal analysis [7–11]. The shrinking unreacted core model is also used [12]. This model includes a temperature dependent diffusion resistance term in the $f(\alpha)$ function.

The available theoretical deductions represent idealistic cases. In reality complicating factors frequently arise that invalidate the assumptions of these models. In our opinion, it is better to determine approximate $f(\alpha)$ functions from the experimental data [13,14] and interpret their features by comparing them to the

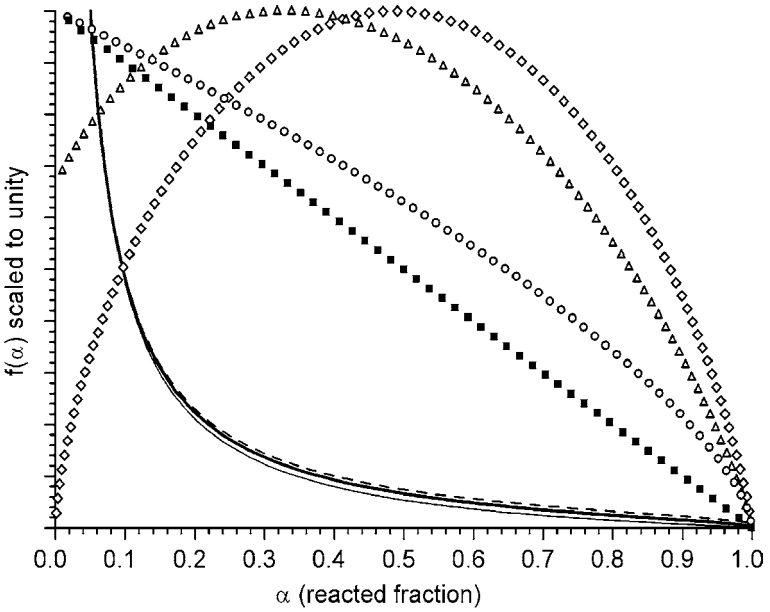

Fig. 1. The $f(\alpha)$ functions deduced from theoretical models: first-order nucleation (Avrami–Erofeev–Mampel model, (◇)), Random pore theory (△), Contracting sphere model (○), first-order kinetics (■), two-dimensional diffusion (- -), three-dimensional diffusion (Ginstling–Brounshtein model, bold solid line), three-dimensional diffusion (Jander model, thin solid line).

theoretical models. We shall follow this approach in the present work. Note that the non-parametric kinetics (NPK) method also provides empirical $f(\alpha)$ functions [15]. However, the NPK method assumes the $f(\alpha)$ function to be exactly the same at different experimental conditions. Unfortunately, this assumption is not always valid in solid phase reactions.

2. Experimental

2.1. Samples

Pieces of Bi_2TeO_5 single crystal grown in air by the Czochralski technique from a Pt crucible were ground in an agate mortar and sieved. The fraction with a grain size smaller than 63 μm was used for the investigations [3].

2.2. Equipment

The thermogravimetric (TG) experiments were carried out by a Mettler TA-1 Thermoanalyser equipped by computerized data acquisition. One charge of the samples was about 100 mg that was measured in an alumina crucible of 5 mm height and 8 mm diameter. The change of the sample mass was below 2.6 mg in each experiment. The powdered samples were compacted by 30 s vibrations before the experiments. Air, pure oxygen, and different argon + oxygen mixtures were used at a flow rate of ca. 75 cm^3/min. The measured TG curves were corrected for the buoyancy effect by measuring 100 mg powdered aluminum oxide under the same experimental conditions.

2.3. Experiments selected for kinetic analysis

Twelve of the experiments presented in reference [3] were analyzed in the present work. Each measurement included a linear heating and an isothermal section [3]. The experimental conditions were chosen so that the set of experiments would allow studying the effect of the heating rate, the temperature of the isothermal section ($T_{isotherm}$), and the partial pressure of oxygen (P_{O_2}), as shown in Table 1. The overall time of an experiment varied between 4 and 20 h, allowing ample time for the dissipation of the high exothermal reaction heat. This later issue has substantial importance

Table 1
Experimental conditions employed for the kinetic analysis

Group	Identifier[a]	Heating rate (°C min^{-1})	$T_{isotherm}$ (°C)	P_{O_2} (kPa)
i	1 (○)	1	670 (1 h)	101
	2 (▽)	2	670 (2 h)	101
	3 (◇)	4	670 (2 h)	101
	4 (△)	10	670 (3 h)	101
ii	5 (□)	10	600 (3 h)	101
	6 (+)	10	625 (3 h)	101
	7 (●)	10	650 (3 h)	101
	4 (△)	10	670 (3 h)	101
	8 (▼)	10	700 (3 h)	101
iii	9 (◆)	4	670 (18 h)	21
	10 (▲)	4	670 (4 h)	46
	11 (■)	4	670 (4 h)	65
	12 (×)	4	670 (4 h)	85
	3 (◇)	4	670 (2 h)	101

The experiments were arranged into three groups for the study of three experimental parameters: heating rate (i); temperature of the isothermal section (ii); and the partial pressure of oxygen (iii).

[a] The symbols in parentheses indicate the line style of the corresponding curves in Figs. 2–8. Experiments 3 and 4 were listed twice in the table since each of them helped studying the effect of two different factors.

in reaction kinetic studies; hence a few characteristic data are listed below. The highest mass-gain rates, observed in short time intervals in the vicinity of the DTG peaks, varied between 10^{-4} and 10^{-3} mg/s in this study. The reaction heat was found to be −87 J/g when normalized to the initial sample mass [3]. For the estimation of the heat production at the DTG peaks we normalized the reaction heat by the change of the mass during the reaction, obtaining −3400 J/g. In this way the highest heat production rates were calculated to be between 0.34 and 3.4 mW in the series of experiments evaluated. Note that the reaction heat is much lower than the usual reaction heats of the oxidation of solid fuels and other organic materials, while the change of the sample mass (<2.6 mg) and the magnitude of the mass change rate peaks (10^{-4} and 10^{-3} mg/s) are similar to or lower than the corresponding values in the reaction kinetic investigation of solid fuels (see e.g. [13,14]).

2.4. Calculations

The experimental data were processed by FORTAN 90 and C^{++} programs developed by one of the authors [13,14,16]. More emphasis was placed on the safety of the iterations than on the computational speed. The differential equations of the models were solved along the experimental $T(t)$ functions by an adaptive stepwise Runge Kutta method [17]. The least squares parameters were determined by the simplex search method [17], which works reasonably on irregular surfaces, too. Each minimization was repeatedly restarted from the optimum found in the previous run of the simplex algorithm until no further improvement was reached, as described by Press et al. [17]. Some of the evaluations proved to be ill-conditioned, requesting parameter transformations [16] and the solution of the differential equations with a very high relative precision (10^{-10}).

3. Results and discussion

3.1. The chemical reaction

The considered oxidation states were 3+ for bismuth and Te^{4+} and Te^{6+} for tellurium. Raman spectroscopic investigation showed that the amount of the excess oxygen was detectable but not remarkable in good-quality Bi_2TeO_5 crystals [18]. Accordingly, the $Bi_2TeO_5 + 1/2O_2 = Bi_2TeO_6$ reaction was assumed. The role of the reverse reaction (Bi_2TeO_6 decomposition) is negligible at $T \leq 670$ °C [3].

3.2. Kinetic model

Eq. (1) was used with empirical $f(\alpha)$ functions determined by the kinetic evaluation. The following approximate formula was used for this purpose [13]:

$$f(\alpha) \cong \frac{(\alpha + z)^a (1-\alpha)^b}{F} \tag{2}$$

Here, $a \geq 0$, $b > 0$ and $z > 0$ are empirical parameters to be determined from the least squares evaluation of the experiments. F is a normalizing factor defined so that max $f(\alpha)$ would be 1. Differentiation of Eq. (2) yields the α_{max} values at which $f(\alpha)$ has its maximum:

$$\begin{aligned} \alpha_{max} &= \frac{(a - bz)}{(a + b)} \quad (a - bz \geq 0) \\ \alpha_{max} &= 0 \quad (a - bz < 0) \end{aligned} \tag{3}$$

This relationship helps to calculate normalizing factor F, and also indicates that Eq. (2) can approximate a wide variety of $f(\alpha)$ functions. Test calculations showed that Eq. (2) can well approximate the curves shown in Fig. 1. The only exception is that Eq. (2) cannot mimic functions starting at infinity. Infinite reaction rates, however, do not arise in thermogravimetric experiments; $f(0) = \infty$ values result from the simplifying assumptions of the classical models of diffusion control [4]. Several theoretical models give $f(0) = 0$ values. From a mathematical point of view this is an error [19], since the only solution of Eq. (1) at $f(0) = 0$ is $\alpha(t) \equiv 0$. In the present work, the $f(0) > 0$ condition was achieved by following constraint:

$$z \geq 10^{-7} \tag{4}$$

At $a = 0$ Eq. (2) reduces to the frequently used $f(\alpha) = (1 - \alpha)^b$ approximation.

The sample mass was normalized by the initial sample mass (m_0), yielding $m^{\text{obs}}(t)$ functions with $m^{\text{obs}}(0) = 1$. The theoretical (stoichiometric) value of the end point is 1.0256 for the $Bi_2TeO_5 \rightarrow Bi_2TeO_6$ reaction in this scale. Accordingly, we can assume that the model should yield theoretical $m^{\text{calc}}(t)$ functions running from $m^{\text{calc}}(0) = 1$ to $m^{\text{calc}}(\infty) = 1.0256$. These boundary conditions provided the following relationship between $m^{\text{calc}}(t)$ and α:

$$m^{\text{calc}}(t) = 1.0256 - 0.0256(1 - \alpha) \tag{5}$$

3.3. Reasons to employ non-linear least squares evaluation techniques

Several linearization techniques are used for kinetic evaluation in the literature of thermal analysis. Most of them are not true least squares methods since they do not allow the separation of simulated and experimental quantities for a true least squares sum. Besides, the transformations resulting in linear relationships has highly uneven sensitivity on the experimental uncertainties of the data [19]. Another important problem is that the linearization methods are restricted to linear and/or isothermal temperature programs. The experiments obtained at linear $T(t)$ programs frequently do not give enough information on the shape of the $f(\alpha)$ curves. The isothermal evaluation has also problems. In thermal analysis, the reaction usually starts before reaching the isothermal section. Important information is lost if the evaluation is restricted only to the isothermal section.

At the present development of computers, the non-linear method of least squares does not involve technical difficulties. One of their advantage is that they can be employed at any $T(t)$ temperature programs. Non-linear least squares methods for kinetic evaluation have been used in thermal analysis for more than 30 years. Broido and Weinstein employed an analogue computer for non-linear parameter optimization in their pioneering work [20]. Later, general purpose numerical algorithms were published that allowed kinetic evaluations by models more complicated than Eq. (1) at arbitrary temperature programs. The first such work, published 23 years ago, was based on computers with 64 kB memory [21]. The listing of all thermoanalytical papers with non-linear least squares evaluation is out of the scope of the present work. A few of them, however, are included in the references [13,14,16,20–24].

3.4. Non-linear least squares evaluation

Three evaluation strategies were used that will be outlined in Section 3.5. In the present paragraph we summarize their technical background. When each experiment was evaluated independently from the other, the following sum was minimized:

$$s = \sum_{i=1}^{N} \frac{[m^{\text{obs}}(t_i) - m^{\text{calc}}(t_i)]^2}{N} \tag{6}$$

Here, t_i denotes the time values in which a digitized m^{obs} value was taken, and N is the number of the t_i points. In this work N lied between 650 and 900. The minimization of Eq. (6) resulted separate E, A, a, b and z values for each experiments. An additional condition, $E \geq 20$ kJ/mol was introduced into the minimization to avoid convergence to unreasonably low E values. The fit of the curve was characterized by the following quantities:

$$\text{fit}(\%) = 100 s^{0.5} \tag{7}$$

When a common E value was searched for the whole set of experiments, the least squares sum was formed for 12 TG curves:

$$S = \sum_{j=1}^{12} \sum_{i=1}^{N_j} \frac{[m_j^{\text{obs}}(t_i) - m_j^{\text{calc}}(t_i)]^2}{N_j} \tag{8}$$

In this case the minimization of S provided a common E value and 12 different values for A, a, b and z (49 parameters altogether). Technically, it was carried out so that E was increased by 1 kJ/mol steps in a wide interval and all experiments were evaluated at each E value as fixed parameter by minimizing Eq. (6). This approach is faster and safer than the simultaneous change of 49 unknown parameters. Sum S was calculated at each E value. The parameter set giving the lowest S was accepted.

3.5. Evaluation strategy I: independent evaluation of the experiments

The first-step of the analysis was the independent (one-by-one) evaluation of the experiments. An earlier work [14] has shown that this approach is ill-defined from a mathematical point of view, since a simple TG curve (i.e. a curve not exhibiting multiple steps) cannot define well five unknown parameters. Accordingly, the resulting E and A values showed a large scattering, as shown in Table 2. In this table, means and standard deviations are displayed for the fit (defined by Eq. (7)), the activation energy, and the logarithm of A/P_{O_2}. The division of A by P_{O_2} serves as normalization, and will be discussed in a later section. The logarithm in the tables is used to be in accord with many other papers in the field. It is well known that there is a linear relationship between E and the logarithm of A. We also observed it with a regression coefficient of 0.98. In our case, however, this correlation does not have physical meaning; it reflects only that the fit to the experimental data mathematically requires the compensation of any error in an E value by a linearly correlated change of $\ln A$ and vice versa (see reference [22] for a detailed analysis of this question). The obtained $f(\alpha)$ functions will be discussed in a later session.

Table 2
Comparing the results of the kinetic evaluation by strategies I–III

Evaluation strategy	I	II	III
Average fit (%)	0.016	0.019	0.013
Standard deviation of fit	0.007	0.007	0.006
Average E (kJ mol^{-1})	39	38	35
Standard deviation of E	19	–	–
$\log_{10}(A/P_{O_2})$ (s kPa)$^{-1}$	−3.53	−3.57	−3.85
Standard deviation of $\log_{10}(A/P_{O_2})$	1.15	0.22	0.21

3.6. Evaluation strategy II: common E value for the whole set of experiments

The easiest solution of the problem outlined above is the decrease of the number of unknown parameters. Accordingly, we evaluated the experiments by assuming a common E value for the whole set of experiments. This procedure decreased the number of unknowns from 60 (5×12) to 49 ($4 \times 12 + 1$), as described in Section 3.4. Table 2 shows that strategies I and II yield approximately the same mean values of E and $\log_{10}(A/P_{O_2})$. The scattering of the $\log_{10}(A/P_{O_2})$ values is 0.22. The fit between the observed and calculated curves is shown in Fig. 2. It is slightly worse than in the case of strategy I.

3.7. Evaluation strategy III: least squares baseline correction

The baseline of a TG experiment changes slowly during an experiment and this change is not perfectly reproducible. The subtraction of an experimental baseline curve, as described in Section 2, improved the precision of the measurements, but did not eliminated completely the baseline uncertainties. Fig. 2 shows that curves (○) and (▽) go above the theoretical limit of $m(\infty) = 1.0256$ (i.e. the mass gain is more than 2.56%). Other plots with zoom on the initial parts of the curves revealed that curves (■) and (×) start with slightly descending sections due to minor baseline problems.

We propose a baseline correction method that can be employed at any least squares kinetic evaluation of TG curves. Recent round-robin studies revealed that baseline problems frequently appear in thermogravimetric studies [23,24] (see e.g. Figs. 1 and 2 of reference [23] and in Fig. 2 of reference [24]). Accordingly, this method is hoped to help other investigators, as well.

The baseline uncertainty, $\delta m(t)$, is approximated by a linear line starting from $\delta m(0) = 0$ and ending at a $\delta m(t_N)$ value, where t_N is the time in the last evaluated point:

$$\delta m(t) \cong \frac{\delta m(t_N)}{t_N} t \tag{9}$$

The correction can be made either by subtracting $\delta m(t)$ from the experimental data, or by adding it to the calculated data. We chose the later way. Accordingly,

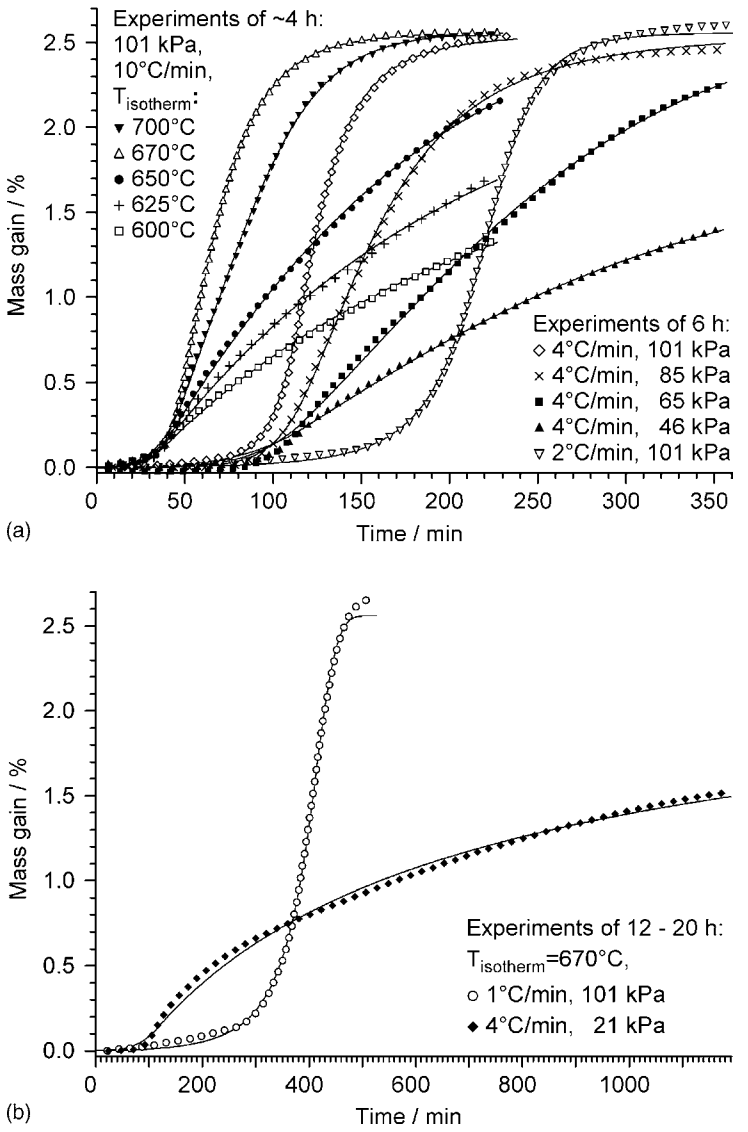

Fig. 2. Simultaneous kinetic evaluation of 12 experiments using evaluation strategy I. (a) Experiments with overall duration of 4–6 h. (b) Experiments longer than 6 h ($t = 0$ corresponds to $T = 200\,^{\circ}\mathrm{C}$). The domain below 200 °C is not shown in the figure.

Eq. (5) was modified to

$$m^{\mathrm{calc}}(t) = 1.0256 - 0.0256(1-\alpha) + \delta m(t) \qquad (10)$$

The values $\delta m(t_N)$ in Eq. (9) are unknown parameters that were determined by the method of least squares, together with the kinetic parameters. Unconstrained minimizations, however, yielded unreasonably high $\delta m(t_N)$ values. It turned out that we need a way to control the magnitude of the $\delta m(t_N)$ values. Accordingly, the appearance of too high $\delta m(t_N)$ values was suppressed by adding a "penalty" to the least squares sum minimized:

$$S = \sum_{j=1}^{12}\sum_{i=1}^{N_j} \frac{[m_j^{\mathrm{obs}}(t_i) - m_j^{\mathrm{calc}}(t_i)]^2}{N_j} + \lambda \sum_{j=1}^{12} [\delta m_j(t_{N_j})]^2 \qquad (11)$$

Here, the $m_j^{\mathrm{calc}}(t)$ functions contain the $\delta m(t)$ baseline corrections through Eq. (10) and multiplier λ serves to control the force of the penalty for the high $\delta m_j(t_{N_j})$ values. The order of magnitude of λ was gradually increased until reasonable baselines were obtained. This was achieved at $\lambda = 10^{-2}$.

Technically, the calculations were carried out as described in Section 3.4. E was increased by steps of 1 kJ/mol and all experiments were evaluated at each E value. At fixed E values, Eq. (11) can be minimized through the one-by-one minimization of sum

$$s = \sum_{i=1}^{N} \frac{[m^{\mathrm{obs}}(t_i) - m^{\mathrm{calc}}(t_i)]^2}{N} + \lambda \sum_{j=1}^{12} [\delta m_j(t_{N_j})]^2 \tag{12}$$

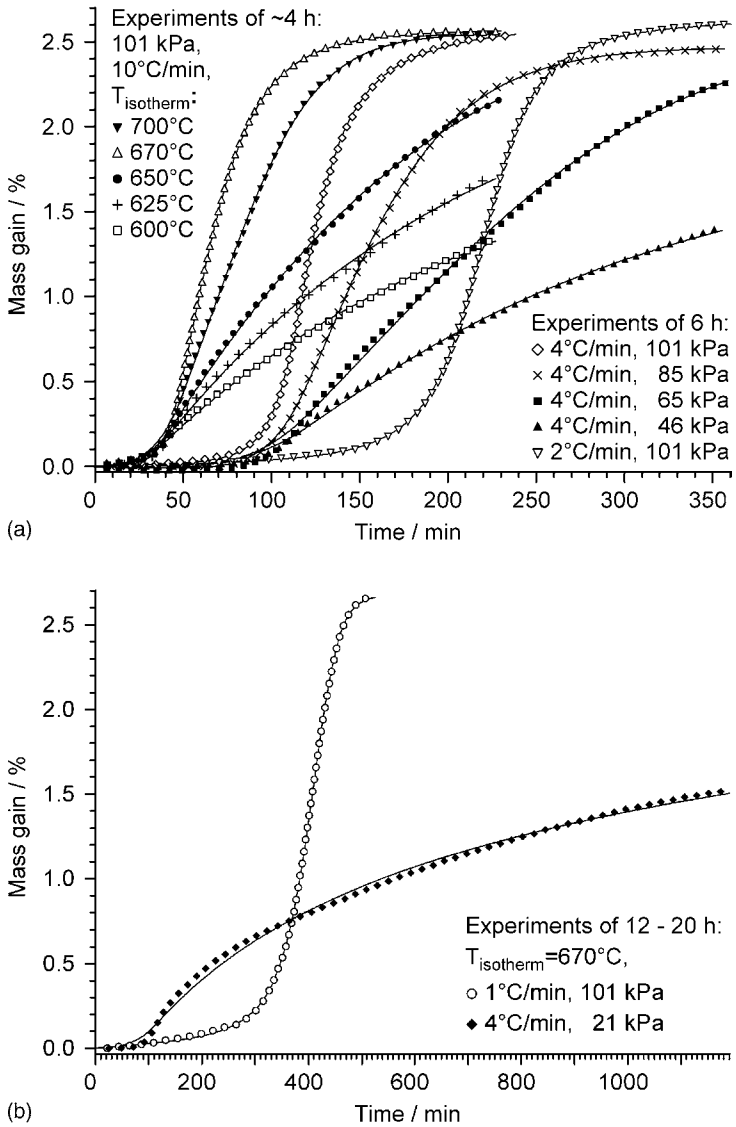

Fig. 3. Simultaneous kinetic evaluation of 12 experiments using evaluation strategy III. (a) Experiments with overall duration of 4–6 h. (b) Experiments longer than 6 h ($t = 0$ corresponds to $T = 200\,^{\circ}\mathrm{C}$). The domain below 200 °C is not shown in the figure.

Table 3
Results of the kinetic evaluation by strategy III

Identifier	Experimental conditions			Results[a]					
	P_{O_2} (kPa)	dT/dt (°C min^{-1})	$T_{isothermal}$ (°C)	Fit (%)	$\log_{10}(A/P_{O_2})$ (s kPa)$^{-1}$	a	b	z	$\delta m(t_N)$
1 (○)	101	1	670	0.008	−3.75	1.06	1.01	0.016	0.0011
2 (▽)	101	2	670	0.005	−3.58	1.16	1.42	0.015	0.0007
3 (◇)	101	4	670	0.008	−3.51	0.92	1.6	0.004	0.0006
4 (△)	101	10	670	0.008	−3.55	0.58	1.18	0.004	0.0001
5 (□)	101	10	600	0.010	−4.07	0	1.48	NA	0.0003
6 (+)	101	10	625	0.016	−4.02	0	1.02	NA	0.0002
7 (●)	101	10	650	0.015	−3.97	0	0.65	NA	0.0000
8 (▼)	101	10	700	0.015	−3.85	3.00	1.02	1.586	−0.0001
9 (◆)	21	4	670	0.024	−3.28	0	2.74	NA	0.0009
10 (▲)	46	4	670	0.014	−3.71	0.27	1.96	0.001	−0.0003
11 (■)	65	4	670	0.025	−3.82	0.24	0.62	10^{-7}	−0.0009
12 (×)	85	4	670	0.008	−3.72	0.52	1.06	10^{-7}	−0.0008

[a] $E = 35$ kJ/mol for all experiments. Value of z is not available when $a \cong 0$.

for each experiment. This procedure is a safer and faster way for the minimization of Eq. (11) than the simultaneous variation of 61 parameters.

The fit obtained in this way is shown in Fig. 3. The means and standard deviations for the fit, E, and $\log(A/P_{O_2})$ are compared in Table 2 to the corresponding values of Evaluation strategies I and II. Table 3 contains a detailed list of the observed parameters.

3.8. Comparison of the obtained $f(\alpha)$ functions

The obtained $f(\alpha)$ functions are displayed in Figs. 4–6, showing the effect of the heating rate, the temperature of the isothermal section and the partial pressure of oxygen, respectively (the arrangement of these figures correspond to groups i–iii in Table 1). Panels (a) and (b) in Figs. 4–6 display the results of evaluation strategies I and III, respectively.

The shape of the obtained $f(\alpha)$ functions evidenced only a slight dependence on the evaluation strategies employed. There is one exception, however, the $P_{O_2} =$ 46 kPa experiment (curve ▲) exhibited different shape in the $\alpha < 0.3$ region in Fig. 6a and b. The $f(\alpha)$ curves shown in Figs. 4–6 can be classified according to their shape:

(1) concave curves with well defined maximum (○, ▽, ◇, △, ▼, ■, ×);
(2) a monotonously decreasing concave curve (●) and an approximately linear curve (+);
(3) convex curves (□, ◆, and curve ▲, at $\alpha > 0.3$).

The maximum curves (group 1) indicate that the reaction accelerates. This phenomenon can be due to an extensive increase of the reaction surface during the conversion. Cracks are formed (as shown earlier by microscopic studies [3]), and in this way the reaction can proceed into the inner part of the particles. A convex $f(\alpha)$ reflects that the reaction is hindered by increasing diffusion control, as the reaction proceeds. Group (2) in the above listing probably represents cases when the accelerating and hindering effects more or less compensate each other.

Fig. 5 compares experiments when various $T_{isotherm}$ temperatures are reached after a relatively fast heating (10 °C/min). High acceleration is observed at $T_{isotherm} = 670$ °C and a less marked one at $T_{isotherm} =$ 700 °C. The difference between the 670 and 700 °C experiments can be due the role of the backward reactions appearing above 670 °C [3].

Fig. 4 displays experiments reaching $T_{isotherm} =$ 670 °C by different heating rates. All curves of the figure exhibit noticeable maximum curve characters. At the slower heating rates (at 1 and 2 °C/min) most of the oxidation occurs during the non-isothermal heating period, as it was shown in Fig. 3 of reference [3]. Accordingly, $f(\alpha)$ functions of maximum curve type also appear during a slow non-isothermal heating. It is possible that the continuously changing temperature bring about mechanical stress in the samples that favor the formation of cracks in the particles.

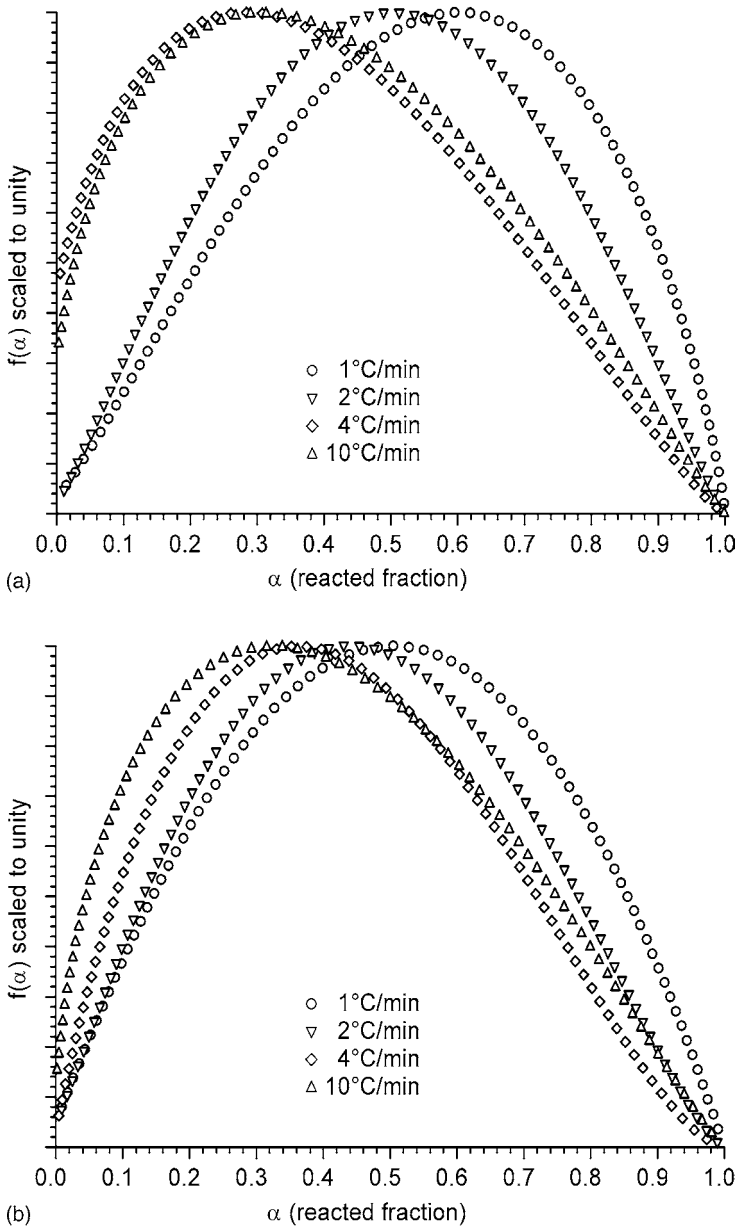

Fig. 4. Effect of the heating rate on the shape of the $f(\alpha)$ functions at $P_{O_2} = 101\,\text{kPa}$ and $T_{\text{isothermal}} = 670\,^{\circ}\text{C}$. Panels (a) and (b) display the results of evaluation strategies I and II, respectively.

Fig. 6 shows the effect of oxygen partial pressure. The convex $f(\alpha)$ at $P_{O_2} = 21\,\text{kPa}$ clearly shows a marked diffusion control. The beginning of the $f(\alpha)$ at 46 kPa could not been determined unambiguously, as mentioned above. At $\alpha \geq 0.12$, however, all the three evaluation strategies yielded monotonously decreasing $f(\alpha)$ at $P_{O_2} = 46\,\text{kPa}$. The $f(\alpha)$ functions at $P_{O_2} = 65$, 85 and 101 kPa have maximum curve characteristics. It is not surprising that lower oxygen partial pressures result in higher diffusion control.

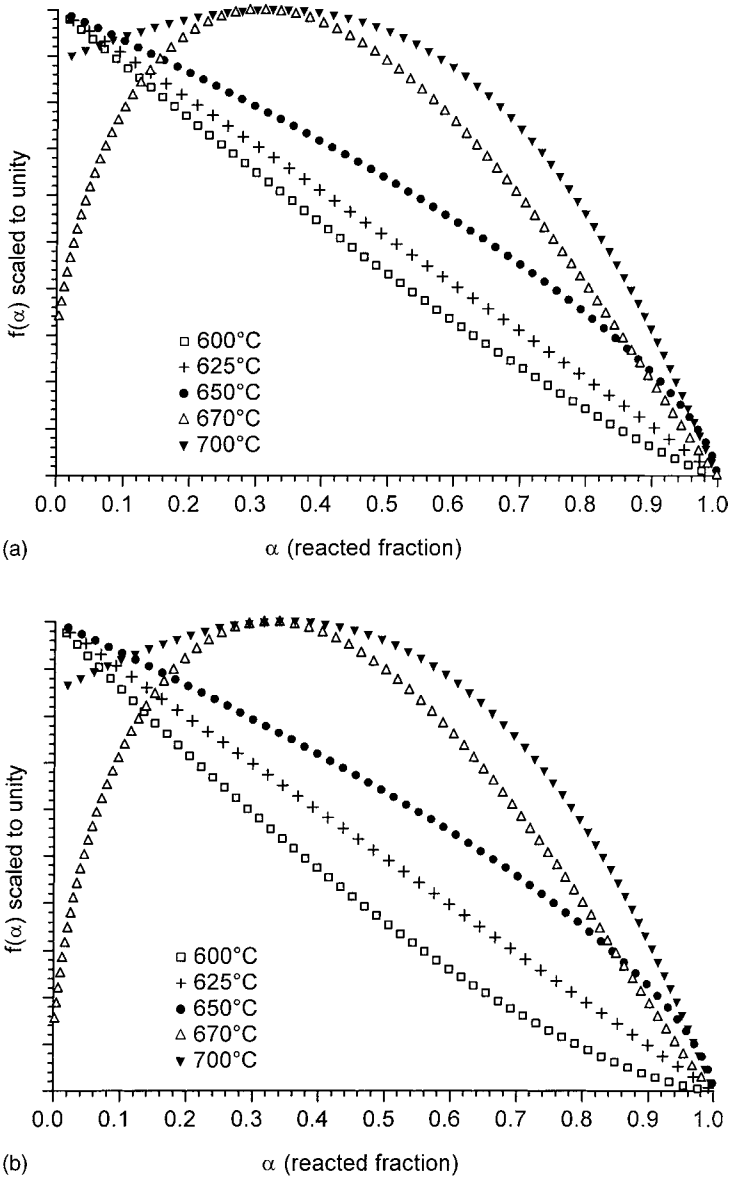

Fig. 5. Effect of the isothermal temperature on the shape of the $f(\alpha)$ functions at 10 °C/min heating rate and $P_{O_2} = 101$ kPa. Panels (a) and (b) display the results of evaluation strategies I and II, respectively.

The peculiarity of this figure is the marked change in the character of the $f(\alpha)$ functions. It can probably be connected to crack formations at higher reaction rates. One can assume that more mechanical stress cumulates in the particles at higher reaction rates, due partly to the higher molar volume of the product phase [25,26] and partly to the effect of the high reaction heat in the vicinity of the reaction surface (note that only the local effect of the reaction heat should be considered). The overall rate of the heat production is low, as outlined in Section 2.

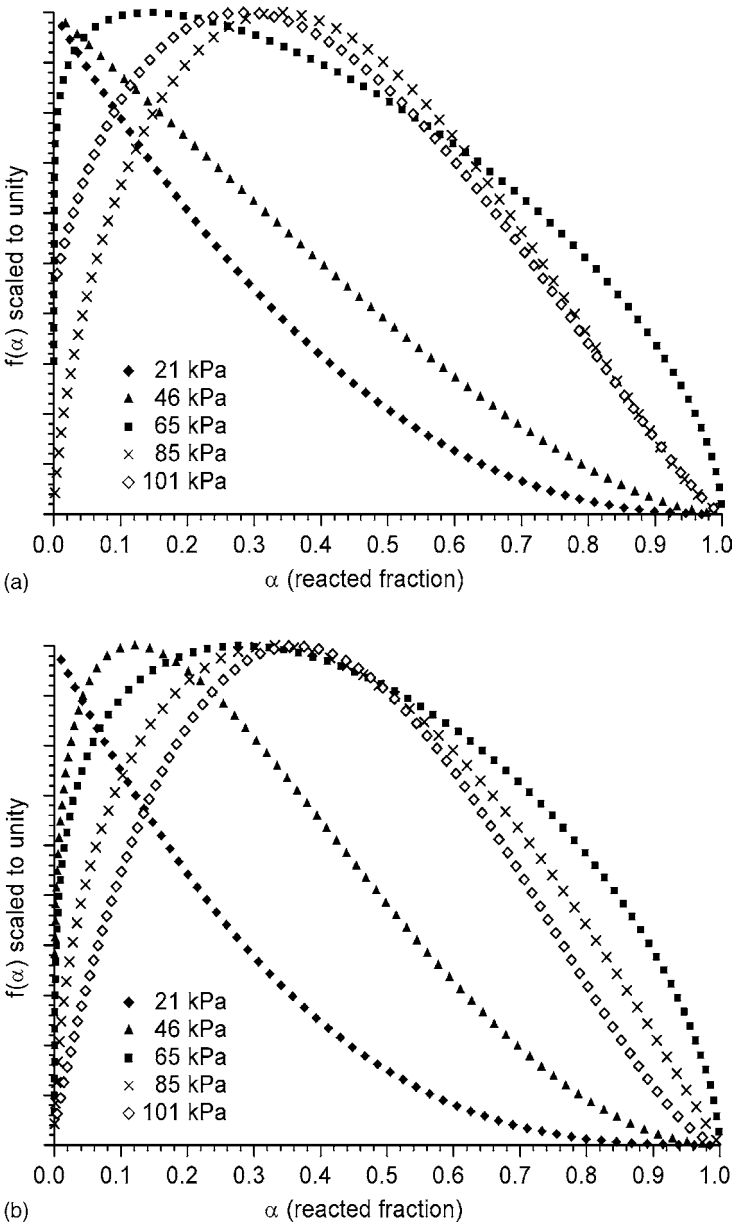

Fig. 6. Effect of the oxygen partial pressure in the ambient gas on the shape of the $f(\alpha)$ functions at 4 °C/min heating rate and $T_{\text{isothermal}} = 670\,^{\circ}\text{C}$. Panels (a) and (b) display the results of evaluation strategies I and II, respectively.

3.9. Additional remarks on the kinetic parameters

In case of oxidation reactions it is an interesting question how does the reaction rate depend on P_{O_2}. The analysis of the $f(\alpha)$ functions, however, revealed that the actual rate is strongly influenced by other factors as well. Accordingly, we cannot determine a well-defined reaction order in respect to P_{O_2}. When the kinetic modeling is based on Eq. (1) and the $f(\alpha)$ function is normalized to unity, the factor containing

Table 4
Dependence of the log A values resulting from evaluation strategy III on the partial oxygen pressure and on the shape of the $f(\alpha)$ curves[a]

Group of experiments	Mean $\log_{10} A$	Mean $\log_{10}(A/P_{O_2})$	Mean $\log_{10}(A/P_{O_2}^{0.5})$
$P_{O_2} = 101$ kPa	−1.78	−3.79	−2.78
$P_{O_2} < 101$ kPa	−1.95	−3.63	−2.79
$f(\alpha)$ is maximum curve	−1.72	−3.68	−2.70
$f(\alpha)$ monotonously decreases[b]	−2.01	−3.81	−2.91

[a] Dimensions: A in s^{-1}, P_{O_2} in kPa.
[b] The $f(\alpha)$ represented by symbol (▲) in Fig. 6 was also included into this group.

P_{O_2} merges into the preexponential factor. If the reaction rate is proportional to the nth power of P_{O_2}, and no other factor influences the value of A, then $A/P_{O_2}^n$ is constant. In our case, however, other factors affecting A do appear, hence we cannot expect an exact A/P_{O_2} = constant relationship. As a very rough approximation, we can study what is the difference between the average $\log_{10}(A/P_{O_2}^n)$ values of the $P_{O_2} = 101$ and $P_{O_2} < 101$ kPa experiments at different n values (such comparisons, however, can be made only at evaluation strategies II and III, since the high scatter of E in the results of evaluation strategy I involves a high scatter in A, as well). This highly approximate approach resulted in $n \approx 0.5$, as shown in Table 4.

We also showed in Table 4 that the average $\log_{10}(A/P_{O_2}^n)$ is lower at monotonously decreasing $f(\alpha)$ functions than at the accelerating cases. This relationship does not depend on the choice of n, as the values at $n = 0$, 0.5 and 1 indicate (perhaps since both $f(\alpha)$ groups contains experiments with $P_{O_2} = 101$ as well as $P_{O_2} < 101$ kPa).

Table 4 displays the results of evaluation strategy III. However, the same relationships were found between the results of evaluation II, too.

3.10. Approximation by a common f(α) function

In the calculations outlined above, the shape of the resulting $f(\alpha)$ functions showed a marked variation on the experimental conditions. It may be interesting to check whether the assumption of identical $f(\alpha)$ for all experiments can also provide an acceptable description for our data. For this test the least squares sum of the whole data set (Eq. (8)) was minimized by

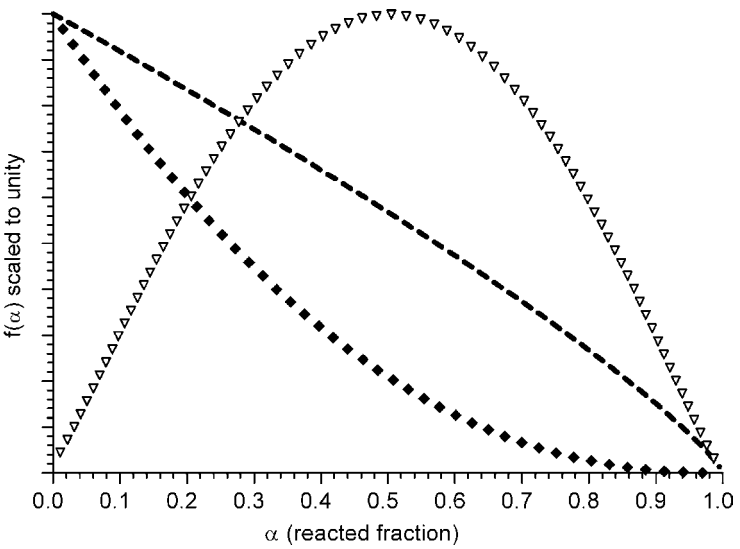

Fig. 7. The $f(\alpha)$ obtained by assuming identical a, b and z for all experiments (- - -). Two other $f(\alpha)$ functions determined by evaluation strategy I for experiment 2 (▽) and 9 (◆) are shown to illustrate the range of the $f(\alpha)$ functions obtained in the paper.

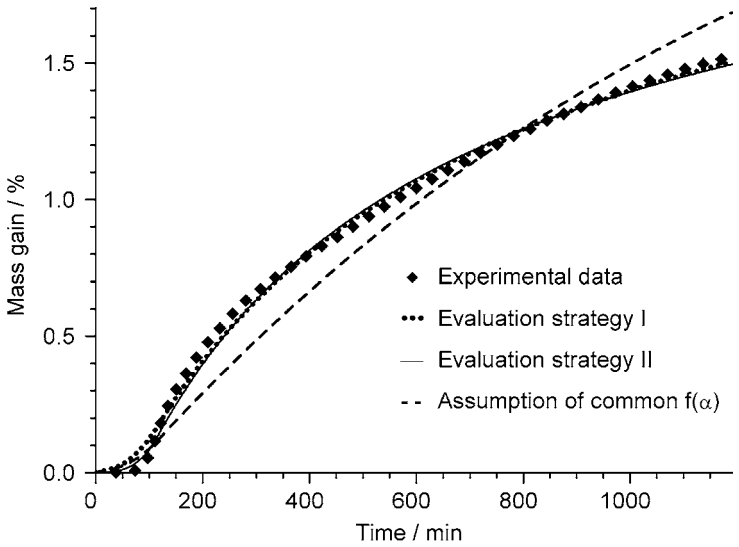

Fig. 8. The assumption of identical *a*, *b* and *z* for all experiments resulted in a particularly bad fit between the observed (◆) and calculated (- - -) $m(t)$ curves of experiment 9. The results of evaluation strategies I (···) and II (—) are shown for comparison.

assuming identical *a*, *b* and *z* parameters for all experiments. *A* and *E* were allowed to have different values in these calculations. The resulting $f(\alpha)$ (the dashed line in Fig. 7) appears to be somewhere around the middle of the range of the concave and convex $f(\alpha)$ functions presented in the above sections. In Fig. 7 the range of the $f(\alpha)$ functions is illustrated by the $f(\alpha)$ functions obtained by evaluation strategy I for experiment 2 (▽) and 9 (◆). The average fit between the experimental and calculated data, 0.039, was much worse than the corresponding values of strategies I (0.16), II (0.19) and III (0.13). The fit was particularly bad in the case of experiment 9, as shown in Fig. 8. The values of *E* in this test exhibited a very high scattering, between 20 and 129 kJ/mol. An attempt to eliminate this scattering by assuming identical *E* for all experiments further worsened the fit, from 0.039 to 0.060. Accordingly, the assumption of a common $f(\alpha)$ can be regarded only as a very rough approximation of the real complexity of the processes.

4. Conclusions

The kinetics of the $Bi_2TeO_5 + \frac{1}{2}O_2 = Bi_2TeO_6$ reaction was described by a model containing empirical $f(\alpha)$ function for the dependence of the reactivity on the conversion of the sample. A series of 12 thermogravimetric experiments were evaluated by three different evaluation strategies. Strategy I allowed each experiment to have its own kinetic parameters. The shape of the resulting $f(\alpha)$ functions showed a marked variation on the experimental conditions. Essentially the same variation of the $f(\alpha)$ functions was observed when the number of unknown parameters was decreased by assuming identical *E* for all experiments in strategy II, and when the baseline uncertainties of the long thermogravimetric experiments were mathematically corrected in strategy III. These observations confirmed the reliability of the results.

The low activation energy values obtained (35–39 kJ/mol) indicate that the rate limiting factors are connected to diffusion and other physical processes with moderate temperature dependence. The analysis of the $f(\alpha)$ functions revealed a complex kinetic behavior influenced by the diffusion of oxygen through the formed products and the accelerating effect of internal surfaces. Monotonously decreasing $f(\alpha)$ functions were observed in two different cases: (i) at $T_{\text{isothermal}}$ of 600–650 °C; (ii) at the oxygen partial pressures below ca. 50 kPa. Experimental conditions leading to relatively high reaction rates (at $T > 650$ °C and P_{O_2} above ca. 50 kPa) favor $f(\alpha)$ functions starting with an increasing section and reaching a maximum around

$\alpha \approx 0.3$–0.5. Non-isothermal experimental conditions also led to similar $f(\alpha)$.

Acknowledgements

This work was supported by the Hungarian Research Found OTKA (Grants T025347, T026647, T029756).

References

[1] I. Földvári, H. Liu, R.C. Powell, Á. Péter, Investigation of the photorefractive effect in Bi_2TeO_5, J. Appl. Phys. 71 (1992) 5465–5473.
[2] Á. Péter, O. Szakács, I. Földvári, L. Bencs, A. Munoz, Dopants in photorefractive bismuth tellurite Bi_2TeO_5 crystals, Mater. Res. Bull. 31 (1996) 1067–1073.
[3] L. Pöppl, I. Földvári, G. Várhegyi, Oxidation of bismuth tellurite, Bi_2TeO_5. Part I. Thermoanalytical and optical microscopic studies, J. Solid State Chem. 161 (2001) 365–372.
[4] W.E. Brown, D. Dollimore, A.K. Galwey, Reactions in the solid phase, in: C.H. Bamford, C.F.H. Tipper (Eds.), Comprehensive Chemical Kinetics, vol. 22, Elsevier, Amsterdam, 1980.
[5] S.K. Bhatia, D.D. Perlmutter, A random pore model for fluid–solid reactions. Part I. Isothermal kinetic control, AIChE J. 26 (1980) 379–387.
[6] J.-L. Su, D.D. Perlmutter, Effect of pore structure on char oxidation, AIChE J. 31 (1985) 973–981.
[7] Z.D. Zivkovic, J. Šesták, Kinetics and mechanism of the oxidation of molybdenum sulphide, J. Therm. Anal. Calorim. 53 (1998) 263–267.
[8] E. Torres García, A. Peláiz Barranco, C. Vázquez, F. Calderón Piñar, O. Pérez Martínez, Oxidation kinetic study of copper(I) in ferroelectric ceramic [$PbTiO_3$–$PbZrO_3$–$PbCuNbO_3$ + 0.5 mol% MnO_2] system, Thermochim. Acta 372 (2001) 39–44.
[9] El.-H.M. Diefallah, M.A. Gabala, A.A. El-Bellihi, N.A. Eissa, Nonisothermal decomposition of CdC_2O_4–FeC_2O_4 mixtures in air, Thermochim. Acta 376 (2001) 43–50.
[10] M. Jablonski, A. Przepiera, Estimation of kinetic parameters of thermal oxidation of ilmenite, J. Thermal Anal. Calorim. 66 (2001) 617–622.
[11] A. Malecki, M. Wierzbicka, Thermal oxidation kinetics of $Ni_{100-x}P_x$ powders, J. Therm. Anal. Calorim. 65 (2001) 367–372.
[12] K. Qiu, T. Mattisson, B.-M. Steenari, O. Lindqvist, Thermogravimetric combined with mass spectrometric studies on the oxidation of calcium sulfide, Thermochim. Acta 298 (1997) 87–93.
[13] G. Várhegyi, P. Szabó, E. Jakab, F. Till, J.-R. Richard, Mathematical modeling of char reactivity in Ar–O_2 and CO_2–O_2 mixtures, Energy Fuels 10 (1996) 1208–1214.
[14] G. Várhegyi, P. Szabó, E. Jakab, F. Till, Least squares criteria for the kinetic evaluation of thermoanalytical experiments. Examples from a char reactivity study, J. Anal. Appl. Pyrolysis 57 (2001) 203–222.
[15] J. Sempere, R. Nomen, R. Serra, J. Soravilla, The NPK method, An innovative approach for kinetic analysis of data from thermal analysis and calorimetry, Thermochim. Acta 388 (2002) 407–414.
[16] G. Várhegyi, E. Jakab, M.J. Antal Jr., Is the Broido—Shafizadeh model for cellulose pyrolysis true? Energy Fuels 8 (1994) 1345–1352.
[17] W.H. Press, B.P. Flannery, S.A. Teukolsky, W.T. Vetterling, Numerical Recipes, The Art of Scientific Computing, 2nd ed., Cambridge University Press, Cambridge, UK, 1992 (online Internet edition: http://www.ulib.org/webRoot/Books/Numerical_Recipes).
[18] R.S. Klein, W. Fortin, I. Földvári, G.E. Kugel, Raman spectra in Bi_2TeO_5 as a function of the temperature and the polarization, J. Phys. Condens. Mater. 10 (1998) 3659–3668.
[19] G. Várhegyi, Reaction kinetics in thermal analysis. A brief survey of fundamental research problems, Thermochim. Acta 110 (1987) 95–99.
[20] A. Broido, M. Weinstein, Kinetics of Solid-Phase Cellulose Pyrolysis, in: Wiedemann (Ed.), Proceedings of the Third International Conference on Thermal Analysis, Birkhauser Verlag, Basel, 1971, pp. 285–296.
[21] G. Várhegyi, Kinetic evaluation of non-isothermal thermoanalytical curves in the case of independent reactions, Thermochim. Acta 28 (1979) 367–376.
[22] G. Várhegyi, P. Szabó, M.J. Antal Jr., Kinetics of the thermal decomposition of cellulose under the experimental conditions of thermal analysis. Theoretical extrapolations to high heating rates, Biomass Bioenergy 7 (1994) 69–74.
[23] H.L. Anderson, A. Kemmler, G.W.H. Höhne, K. Heldt, R. Strey, Round robin test on the kinetic evaluation of a complex solid state reaction from 13 European laboratories. Part 1. Kinetic TG-analysis, Thermochim. Acta 332 (1999) 33–53.
[24] M. Grønli, M.J. Antal Jr., G. Várhegyi, A round-robin study of cellulose pyrolysis kinetics by thermogravimetry, Ind. Eng. Chem. Res. 38 (1999) 2238–2244.
[25] D. Mercurio, M. El Farissi, B. Frit, P. Goursat, Étude structurale et densification d'un nouveau matériel piezoélectrique: Bi_2TeO_5, Mater. Chem. Phys. 9 (1983) 467–476.
[26] G.G. Gospodinov, K.M. Gjurova, Synthesis, crystallographic data and thermostability of some metal *ortho*-tellurates of the type of Me_3TeO_6 and Me_2TeO_6, Thermochim. Acta 83 (1985) 243–252.